Automatic Segmentation of Pulmonary Lobes Robust Against Incomplete Fissures

Eva M. van Rikxoort*, Mathias Prokop, Bartjan de Hoop, Max A. Viergever, Josien P. W. Pluim, and Bram van Ginneken

***Abstract*—A method for automatic segmentation of pulmonary lobes from computed tomography (CT) scans is presented that is robust against incomplete fissures. The method is based on a multi-atlas approach in which existing lobar segmentations are deformed to test scans in which the fissures, the lungs, and the bronchial tree have been automatically segmented. The key element of our method is a cost function that exploits information from fissures, lung borders, and bronchial tree in an effective way, such that less reliable information (lungs, airways) is only used when the most reliable information (fissures) is missing. To cope with the anatomical variation in lobe shape, an atlas selection mechanism is introduced. The method is evaluated on two test sets of 120 scans in total. The results show that the lobe segmentation closely follows the fissures when they are present. In a simulated experiment in which parts of complete fissures are removed, the robustness of the method against different levels of incomplete fissures is shown. When the fissures are incomplete, an observer study shows agreement of the automatically determined lobe borders with a radiologist for 81% of the lobe borders on average.**

***Index Terms*—Incomplete fissures, lobes, , pulmonary, registration, segmentation.**

I. Introduction

COMPUTED tomography (CT) is the most sensitive way to image the lungs *in vivo*. Multidetector scanners allow for visualization of the lungs with high anatomical detail. The accurate interpretation of a chest CT scan provides a challenge to radiologists due to the large amount of data: a chest CT scan typically contains over 400 slices. Therefore, automation is essential to extract information from those scans.

The human lungs are divided into five anatomical regions, the pulmonary lobes. Physically, the lobes are separated by a double layer of visceral pleura called the pulmonary fissures. The right lung consists of three lobes: the upper lobe, the middle lobe, and the lower lobe. The left lung consists of two lobes, and does not have a middle lobe. The lobes are separately supplied by the first subdivisions of the bronchial tree after the main bronchi. Since also the vascular, nerve, and lymphatic supply from the hilum to each lobe are mostly separated, the lobes function relatively independently within the lungs. The fissures separating the lobes stem disease spread. When the pulmonary fissures are not complete, lobes are connected. Several studies have shown that incomplete pulmonary fissures are a very frequent phenomenon. Raasch *et al.* [1] inspected 100 lung specimens and found the left major fissure to be incomplete in 46% of the specimens, the right major fissure in 70% of the specimens, and the right minor fissure in 88% of the specimens. Aziz *et al.* [2] found the left major, right major, and right minor fissure to be incomplete of 43%, 48%, and 63% in 622 CT examinations, respectively. In addition, no right minor fissure at all was found in 22% of all cases. Gülsün *et al.* [3] inspected the major fissures in 144 CT scans from disease free subjects and found the left major fissure to be incomplete in 60% of the cases and the right major fissure in 63% of the cases. Complete major fissures in both lungs were only observed in 17% of the cases. Fig. 1 shows an examples of a scan with complete fissures and a scan with incomplete fissures.

Segmentation of the pulmonary lobes is important to localize parenchymal disease inside the lungs and to quantify the distribution of a parenchymal disease. The degree of deterioration can vary substantially between the different lobes. This is for example important for lobe volume reduction in emphysema patients [4]. This treatment has been shown to be significantly more effective in cases of heterogeneously distributed emphysema than in patients with a homogeneous distribution [5]. In cases with incomplete fissures, it is still important to correctly identify the lobes; the disease might not have spread over the different lobes, which indicates the lobes still function independently. Although radiologists might be able to identify lobar boundaries on CT scans, manual delineation of over 400 CT images is unthinkable in clinical routine.

For an automatic lobe segmentation method, the most important information is provided by the pulmonary fissures since they are the physical boundaries between the lobes. Several papers have been published about extracting the pulmonary

Manuscript received October 13, 2009; revised February 09, 2010; accepted February 19, 2010. First published March 18, 2010; current version published June 03, 2010. This work was supported by the Netherlands Organization for Scientific Research (NWO). *Asterisk indicates corresponding author.*

*E. M. van Rikxoort was with the Image Sciences Institute, 3584 CX, Utrecht, The Netherlands. She is now at the Thoracic Imaging Research Group, Department of Radiological Sciences, David Geffen School of Medicine, University of California, Los Angeles, CA 90095 USA (e-mail: evanrikxoort@mednet.ucla.edu).

M. Prokop was with the Department of Radiology, University Medical Center Utrecht, 3584 CX Utrecht, The Netherlands. He is now with the Department of Radiology, Radboud University Nijmegen Medical Centre, 6525 GA, Nijmegen, The Netherlands.

B. de Hoop is with the Department of Radiology, University Medical Center Utrecht, 3584 CX Utrecht, The Netherlands.

M. A. Viergever and J. P. W. Pluim are with the Image Sciences Institute, 3584 CX, Utrecht, The Netherlands.

B. van Ginneken was with the Image Sciences Institute, 3584 CX, Utrecht, The Netherlands. He is with the Diagnostic Image Analysis Group, Department of Radiology, Radboud University Nijmegen Medical Centre, 6525 GA, Nijmegen, The Netherlands.

Color versions of one or more of the figures in this paper are available online at http://ieeexplore.ieee.org.

Digital Object Identifier 10.1109/TMI.2010.2044799

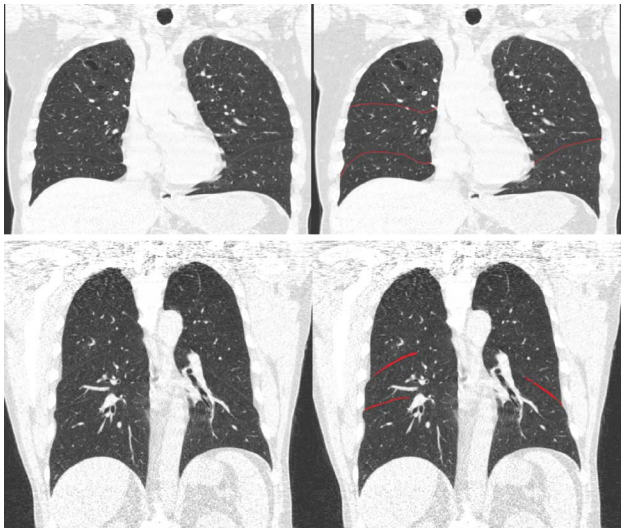

Fig. 1. Example slices of a scan with complete and a scan with incomplete fissures. The first row shows a coronal slice of a scan with complete fissures on the left. The frame on the right shows the segmentation of the fissures. The second row shows a coronal slice and the fissure segmentation for a scan with incomplete fissures. In this case, the lobe borders have to be extrapolated from the fissures.

fissures from chest CT data [6]–[8]. When the fissures are complete, they define the pulmonary lobes and a method to extract the fissures provides enough information to obtain the lobes. However, since fissures are often incomplete or hard to locate automatically, a fissure segmentation is usually incomplete and deriving a lobe segmentation from it is not trivial. In these cases, there are several alternatives that can be used to infer the lobe borders. Important information can be extracted from the segmentation of the lungs since the shape of the lobes is constrained by the shape of the lungs. In addition, the topology of the bronchial tree can be exploited. The different lobes are separately supplied by the first subdivisions of the bronchial tree after the main bronchi. Therefore, given a division of the bronchial tree into its lobar bronchi, a segmentation of the pulmonary lobes can be approximated by assigning each voxel inside the lungs to the lobar label of the nearest bronchus. The pulmonary vessels also provide information since the lobes are supplied with blood by different subtrees of the pulmonary vessel trees. However, in practice there are vessels crossing lobar boundaries in a nonnegligible number of cases. In addition to anatomical information, knowledge about the shape of the various lobes can be used. Radiologists combine all this information when they infer the lobar boundary in a CT scan.

A few papers have been published that not only segment the pulmonary fissures but also extract the lobes [9]–[13]. Kuhnigk *et al.* [9] proposed an interactive 3-D lobe segmentation method that uses the fact that there are fewer vessels around the lobar boundaries. The lobar boundary was first determined by searching for regions in which no (or few) vessels are present. This is combined with the image intensity to include the pulmonary fissures. Next, a watershed transform was applied to segment the lobes. After the watershed transform there is an option to manually correct the lobe segmentation. A disadvantage of this method is that the fissures are not detected, therefore, the method is not guaranteed to follow the fissures where those are present. The performance of the method was not quantitatively evaluated.

Zhang *et al.* [10] proposed a lobe segmentation framework that solely relies on the detection of the fissures. When the fissures were not detected or not present, manual interaction was needed to segment the lobes. Therefore, this method is only able to automatically segment the lobes in cases with complete pulmonary fissures. No evaluation was performed on cases with incomplete fissures.

Pu *et al.* [11] recently proposed a lobe segmentation method capable of handing incomplete fissures. After an initial fissure segmentation and classification of the fissures into major and minor fissures, the individual fissures were extended to the lung boundaries using implicit Radial Basis functions. No anatomical information was used for the extension of the fissures. The method was evaluated on 65 CT scans by visual inspection of two radiologists using a five point score. The results showed that 50.8% of the segmentations were rated as good or excellent by both observers. It was not specified how many of the 65 CT scans used for evaluation contained incomplete fissures.

Ukil and Reinhardt [12] recently presented a method to segment the pulmonary lobes based on information extracted from the fissures and the airways. The fissures were first detected based on a 2-D ridgeness operation on axial slices. When the fissures were detected to be incomplete on a slice, they were extended using a 2-D spline interpolation that employed automatically determined anchor points from a labeled bronchial tree to ensure anatomically correct boundaries. When the anchor points from the bronchial tree did not provide enough information, manual interaction was performed. For the data used in the paper, 25% of the scans needed manual interaction. The method was qualitatively evaluated for cases with incomplete fissures on 10 scans, showing that four of those scans contained no errors. The main disadvantage of this method is that manual interaction is needed in a substantial percentage of scans to obtain an accurate lobe segmentation.

In a previous paper [13], we proposed a lobe segmentation method that used a fissure segmentation and a lung segmentation to segment the lobes using a voxel classification approach. Each voxel inside the lungs was classified as belonging to a certain lobe based on the distance and direction to the segmented fissures and the position inside the lung segmentation. The method is automatic and segments the lobes in cases with incomplete fissures based on the classification results for each voxel. The method was evaluated for a set of 100 scans. Although overall performance was good, the lobe segmentation in scans with incomplete fissures was often incorrect.

In this paper, we present a fully automatic lobe segmentation method that employs the fissures, the lungs, the bronchial tree, and shape information to define the lobe borders. The vessel tree is not used since it is not reliable enough. To investigate the performance and robustness of the method in cases with incomplete fissures, four experiments are performed on 120 chest CT scans in total. To test the robustness of the method at different levels of incomplete fissures, an experiment was set up in which parts of fissures were automatically removed to simulate the fissures being incomplete.

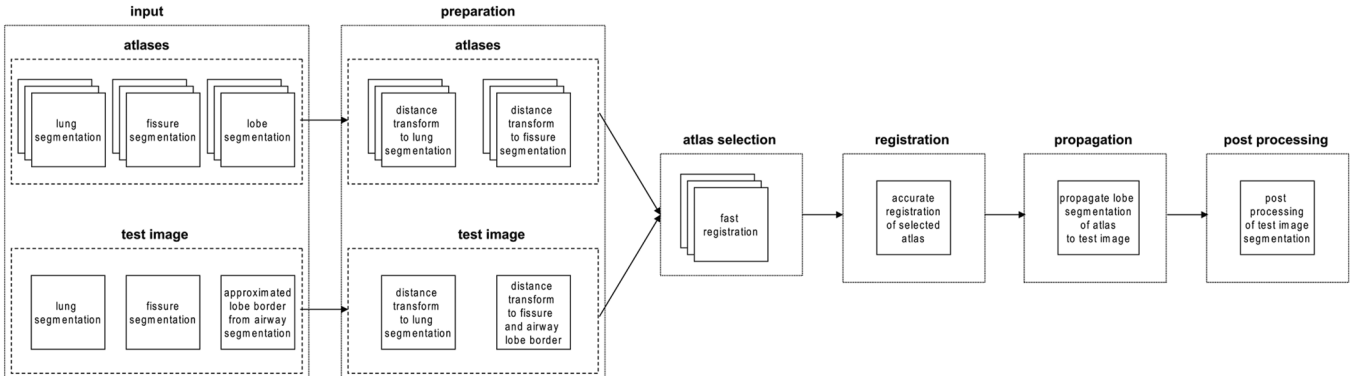

Fig. 2. Flowchart of the method.

II. Method: Overview

A multiatlas lobe segmentation method is developed in which information from scans with complete fissures is transformed to a test scan to obtain a lobe segmentation in the test scan. Atlas-based segmentation starts by registering an atlas with a test image to be segmented. To obtain a segmentation of the test image, a labeling of the atlas is transformed using the mapping determined during the registration. In the case of lobe segmentation, the goal of the registration is to transform the atlas to the test scan in such a way that the lobar borders line up. Directly registering chest CT scans from different subjects does not lead to satisfactory results due to anatomical variations inside the lungs; the fissures do generally not line up after registration. Therefore, we employ anatomical information obtained from the scans by automatic segmentations of the lungs and the fissures. When the fissures in the test scan are not complete, information extracted from a segmentation of the bronchial tree is added to guide the registration.

The method starts by segmenting anatomical structures of interest in the test scan: the lungs, the fissures, and the bronchial tree (Section III). These anatomical structures are used during registration in a multiatlas segmentation approach (Section IV). A flowchart of the method is presented in Fig. 2.

III. Prerequisite Segmentations

The lung, fissure, and bronchial tree segmentations applied in this paper are all based on previous work and are therefore only briefly described here.

A. Lung Border Segmentation

The lung fields are segmented with an automatic 3-D algorithm [14]. From the segmentation of the lungs, the borders of the lungs are extracted as those voxels in the lung segmentation for which at least one of the six-connected neighbors is outside the lung segmentation.

B. Fissure Segmentation

Fissure segmentation is initiated by applying a supervised fissure enhancement filter as described in [7]. This enhancement filter consists of two consecutive k-nearest neighbor classifications and assigns to each voxel a probability that it belongs to a fissure. An example result of the fissure enhancement is shown in Fig. 3. Since we are only interested in the major and minor fissures, i.e., the boundaries between the lobes, the enhanced fissures are converted to a segmentation of the major and minor fissures. To accomplish this, the probabilities resulting from the fissure enhancement are first thresholded at 0.7 to eliminate all voxels with a low probability of being on a fissure. Next, since the fisures are free-form surfaces in the lungs that locally resemble plates, the remaining voxels are grouped into plates using the technique described in [13] and [15]. This method groups neighboring voxels based on their likelihood of constituting a plate given second-order image information.

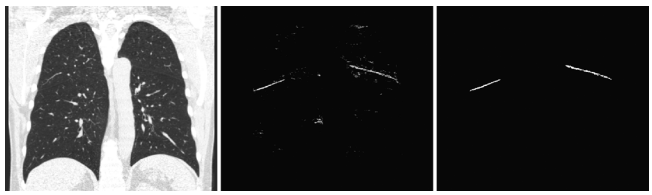

Fig. 3. Example of the fissure segmentation. The left frame shows a coronal CT slice, in the middle frame the result of the fissure enhancement is shown. The last frame shows the binary fissure segmentation.

The grouping of voxels is based on gray-scale curvature information obtained from the eigenvalues of the Hessian matrix. For each voxel, the Hessian matrix is a symmetric matrix that is composed from the six independent second-order derivatives. When performing an eigenvalue analysis of the Hessian matrix, the principal directions ($\hat{v}_0$, $\hat{v}_1$, $\hat{v}_2$) in which the local second-order structure can be decomposed are extracted. The corresponding eigenvalues ($|\lambda_0| \geq |\lambda_1| \geq |\lambda_2|$) are real and denote the second-order derivative in the principal directions. At a fissure, λ_0 is expected to be large since there is a strong curvature perpendicular to the fissure, λ_1 and λ_2 are typically both low.

We employ $\hat{v}_0$ calculated at scale $\sigma = 1$ to group voxels belonging to the same plate. For a voxel v_a, all voxels v_b within a distance d are considered to be on the same plate if 1) the directions of $\hat{v}_0$ are similar for both voxels and 2) the voxels belong to the same plate (and not to parallel plates). The first condition is checked by taking the inner product of the normalized eigenvectors $\hat{v}_0$ at the locations of v_a and v_b; if v_a and v_b have similar orientation the product will be close to one. The minimum value

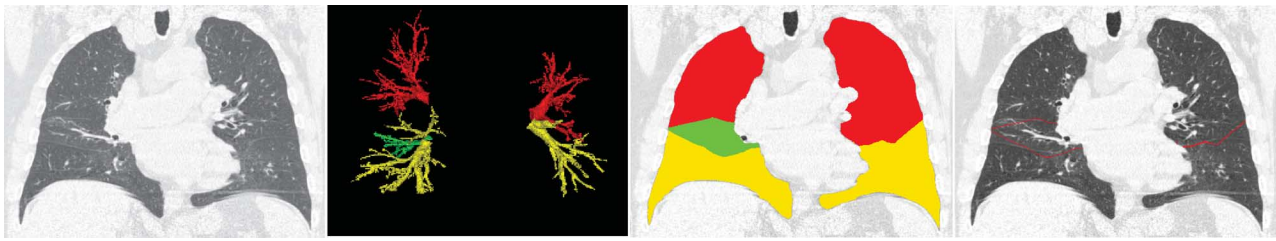

Fig. 4. Illustration of the approximated airway lobes by the labeling of the bronchial tree. The first frame shows the original coronal slice. In the second frame a rendering of the bronchial tree is shown, the different lobes are color coded: red bronchi belong to the upper lobe, yellow bronchi to the lower lobe, and green bronchi to the middle lobe. The third frame shows the approximated lobes by assigning each voxel inside the lungs to the lobe of the closest airway voxel. The last frame shows the approximated lobe borders.

of the inner product is set by a threshold T_v. The second condition is checked by taking the outer product of the normalized difference vector $\hat{w}$ between the locations of v_a and v_b and $\hat{v}_0$ of v_a; if the voxels are on the same plate the outer product will be close to one. A threshold T_w is used to set the mimimum value of the outer product. To discard accessory fissures and spurious detections, only plates with a sufficient size m are retained.

In this paper, the grouping is performed with the following settings: d is set to three voxels, T_v and T_w are both set at 0.985, and m is set to 8000 voxels. The final result of the fissure segmentation is a binary image in which all voxels on the fissures are 1 and all other voxels are 0. An example result of the final fissure segmentation is shown in Fig. 3.

C. Approximated Lobe Borders From an Airway Segmentation

The segmentation of the airway tree will be used to approximate the lobe borders. The airways are automatically segmented using the method described in [16]. Next to a segmentation of the airway tree this method provides the anatomical labels for airway branches up to segmental level. These anatomical labels are transformed into lobar labels by assigning each labeled segmental bronchus to the corresponding lobe. Next, the complete tree is relabeled by assigning to each airway segment the label of the lobar segment from which it branches off. Given these labeled airways, the lobes can be approximated by assigning each voxel in the lungs to the lobar label of the closest bronchus voxel. Approximated lobar boundaries are extracted as those voxels for which one of the six-connected neighbors in the lungs belongs to another lobe. Examples of the segmented and labeled airway tree, and the approximated lobar boundaries can be seen in Fig. 4.

IV. Multiatlas Lobe Segmentation

For the multiatlas lobe segmentation it is assumed that a set of n atlases with complete pulmonary fissures and corresponding segmented lungs, fissures, and lobes is available. The atlases used in this study are specified in Section V-A. For a test scan in which the lungs, fissures, and airways have been automatically segmented, the following steps are performed. 1) The test image and atlases are prepared for registration (Section IV-B). 2) All atlases are registered to the test scan and the most promising atlas is selected for further processing (Section IV-C). 3) The lobes in the test scan are now segmented by accurately registering the selected atlas and propagating the lobe labels with the resulting transformation (Section IV-D), followed by a postprocessing (Section IV-E).

A. Registration Method

The atlas-based lobe segmentation requires two registration methods to be available: a fast (computationally cheap) method which is used to select the atlas that is most similar to the test image, and an accurate (computationally expensive) method which transforms an atlas image to a target image with high accuracy for the final lobe segmentation. Throughout this paper we will refer to these two registration methods as "fast registration" and "accurate registration."

For all experiments in this paper, elastix [17][1] version 3.9 was used for registration. In this paper, the sum of squared differences (SSD) was used as a similarity measure. For both the fast and the accurate registration, images were first roughly aligned with an affine transformation. After that, a nonrigid registration modeled by *B*-splines was performed. For the optimization of the cost function, an iterative stochastic gradient descent optimizer [18] was used. To speed up the registration, a small randomly chosen subset of samples was used in each iteration. To avoid local minima, a multiresolution strategy was taken.

The settings used for registration were determined in pilot experiments. Details about the parameter settings of elastix can be found in [17]. For the affine registration four resolutions were used, in each of which 1000 iterations of the stochastic gradient descent optimizer were performed. For the nonrigid *B*-spline registration five resolutions were used. The *B*-spline grid spacing used in these resolutions was 64, 32, 16, 8, and 4 voxels, respectively. For the fast registration, the optimizer performed 100 iterations in the first three resolutions and 200 iterations in the fourth and the fifth resolution. In each iteration, 2000 random samples were used. For the accurate registration, the optimizer performed 300 iterations in the first two resolutions and 600 iterations in the last three resolutions. In each iteration of the accurate segmentation, 4000 random samples were used.

B. Preparation of Scans for Registration

During registration, the anatomical structures as obtained by the prerequisite segmentations are employed. The registration is performed to two images simultaneously: one image containing the lung border and the other image containing the fissure segmentations. The cost function is calculated as a combination of

[1]elastix can be downloaded from http://elastix.isi.uu.nl.

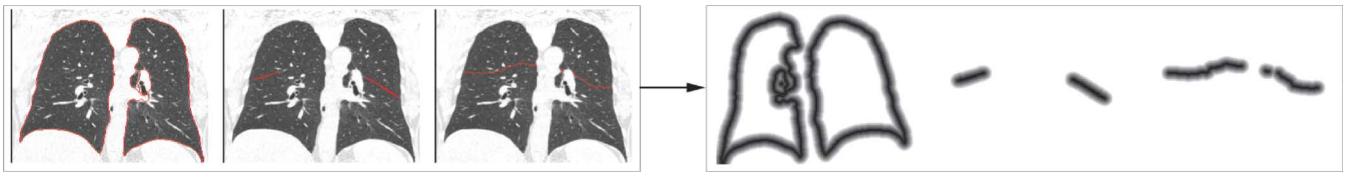

Fig. 5. This figure illustrates the input to the registration method for a test scan. The left panel shows the prerequisite segmentations overlayed on a coronal slice. From left to right: the lung border, fissures, and approximated lobe border from the airways. The second frame shows the distance transforms to the different structures truncated at 14 mm.

both registrations, giving them both equal weight. Since registration involves an optimization towards a minimum of the similarity measure, not the binary segmentations are used as input but the distance transform to those segmentations. This smoothes the cost function and encourages the optimization to gradually converge to the correct position. Exact Euclidean distance is used taking voxel spacing into account [19]. The distance transforms are truncated at 14 mm. The result of this preparation is illustrated in Fig. 5. For the test image, the fissure segmentations are augmented with the approximated lobe border from the bronchial tree only on positions where the fissures are not defined. This is achieved as follows: The distance transforms to the fissures and the approximated lobe borders are calculated separately. Next, the values of the distance transform to the approximated lobe border are blended with the distance transform to the fissures only on those positions where no information from the fissures is available, i.e., further than 14 mm from the fissure segmentation.

Since SSD is used as a cost function, different structures can be given different weights during registration by multiplying their values by a weighting factor. For the lobe segmentation, three parameters are introduced to control the weights of the different structures: ω_f for the fissure, ω_l for the lung border, and ω_b for the bronchial tree. In pilot experiments, suitable values for the different weights were found to be $\omega_f = 4$, $\omega_l = 1$, and $\omega_b = 1$. This setting encourages that the fissures, when available, are most heavily weighted during the registration.

C. Atlas Selection

An atlas selection is performed in which the atlas that is anatomically most similar to the test scan is automatically selected. For this atlas selection, all atlases are registered to the test scan using fast registration. The fissure segmentation that is available for the atlases is transformed to the test scan using the transformation determined during the fast registration. The anatomically most similar atlas for the lobe segmentation of a particular test scan is the scan for which the fissures of the transformed scan line up best with the fissures of the test scan. The atlas with the highest number of voxels of the transformed fissure within 1 mm of the fissure in the test scan is selected to be the most promising atlas for further processing.

D. Lobe Segmentation

The selected atlas is registered to the test image using the accurate registration. To obtain a lobe segmentation for the test image, the lobe segmentation of the atlas is transformed using the mapping determined during the accurate registration.

E. Postprocessing

Since the lung borders of the atlas and the test image are not forced to line up during the registration, postprocessing is necessary to guarantee that every voxel inside the lungs in the test image is assigned to a lobe. Every voxel inside the lung segmentation of the test image that is not assigned to a lobe after the transformation of the atlas lobes, is given the label of the closest voxel in the transformed lobe segmentation.

V. Materials

A. Atlases

A set of five atlases with complete pulmonary fissures was taken from the NELSON study, a Dutch lung cancer screening trial [20]. No other factors than the presence of complete fissures were taken into account for selection of the atlases. Since it is rare to find scans in which all three pulmonary fissures are complete, different atlases were selected for the left and right lung. The scans from the NELSON trial are low dose CT (30 mAs at 120 kV for patients weighing ≤ 80 kg and 30 mAs at 140 kV for those weighing over 80 kg). Data was acquired on Mx8000IDT or Brilliance-16 CT scanners (Philips Medical Systems, Cleveland, OH) in about 12 s in spiral mode with 16×0.75 mm collimation and 15 mm table feed per rotation (pitch $= 1.3$). Axial images of 1.0 mm thickness at 0.7 mm increment were reconstructed using a moderately soft kernel (Philips "B") with the smallest field-of-view that included the outer rib margins at the widest dimension of the thorax. All scans were reconstructed to 512×512 matrices.

The lungs and fissures in the atlases were automatically segmented using the methods described in Section III. The results of the automatic methods were visually checked and edited where needed by a human observer. Since the fissures in the atlas scans were complete, a lobe segmentation was extracted directly from the segmented fissures.

B. Test Data

Two test sets have been used in this paper, which we will refer to as test set A and test set B.

Test set A contains 20 normal dose (120 kV, 100–150 mAs) inspiration CT chest scans of 20 different patients randomly selected from clinical practice at the University Medical Center Utrecht, The Netherlands. Other settings were identical to the data from the NELSON trial (Section V-A).

Test set B consists of 100 low dose scans taken from the NELSON screening trial (see Section V-A). These 100 scans

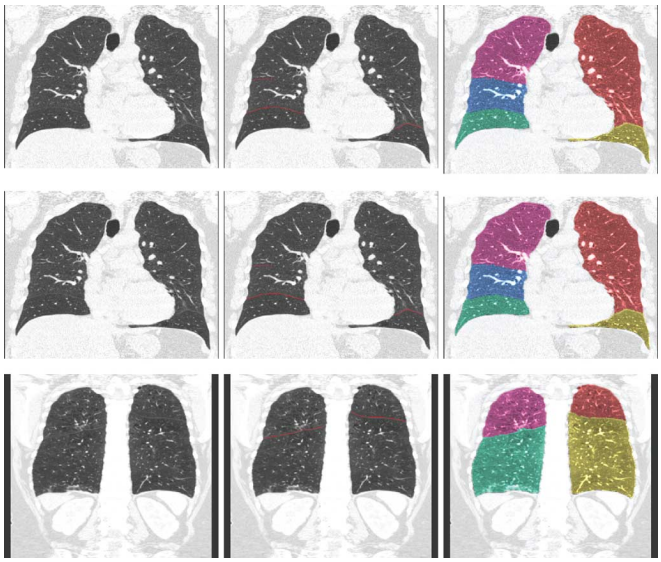

Fig. 6. Example output of the automatic lobe segmentation on three scans taken from test set A. The first column provides the original slice, in the second column the reference standard is shown, in the last column the result of the automatic lobe segmentation is provided.

were selected from a set of 1000 scans to have the most incomplete fissures by visual inspection. In the 100 scans, 56 left major fissures were incomplete, 90 right major fissures were incomplete, and 87 right minor fissures were incomplete.

C. Manual Segmentations

To allow for a quantitative evaluation of the performance when fissures are present, a human observer manually indicated the lobar fissures in every fourth coronal slice for all scans in test set A. The observer was instructed only to indicate the fissures where visible and not to draw the lobe borders where no fissure is available. This resulted in 939 slices with manual segmentations. Since fissures are often hard to distinguish using only 2-D information, observers scrolled through the scan in the axial and sagittal direction before segmenting the fissures on the coronal slices, and indicated marker points on each individual fissure. These points were visible in the coronal direction while segmenting the fissures. Segmenting fissures was performed by clicking points on the fissure; between two points, a straight line was automatically drawn. This line was refined using the Hounsfield values in a small neighborhood perpendicular to the line. Each voxel on the straight line between two manually indicated points was moved at most one voxel in the perpendicular direction to a voxel with a higher Hounsfield value. This refinement was necessary to accurately segment the centerlines of the fissures. Examples of the data used and the manual segmentations can be seen in Fig. 6.

VI. Experiments

To evaluate the performance of the automatic lobe segmentation, five different experiments were performed.

1) For test set A, the performance of the lobe segmentation method was quantitatively evaluated by comparing it to the manual reference standard. Three measures were calculated: root mean square (rms), mean, and maximum distances between the manually defined fissures and the nearest point on the automatically determined lobe border. Since manual tracings are only available for the fissures and not for the lobe borders where no fissure is available, the distance measures compute the minimum distance of a point on the manual segmentation to a point on the automatic segmentation. This approach is the same as described in [12]. The result of this evaluation indicates how well the lobe segmentation performs on positions where a fissure is available.
2) To quantify the robustness of the automatic lobe segmentation at different levels of incomplete pulmonary fissures, a separate evaluation was performed on a subset of test set A which showed (nearly) complete pulmonary fissures for one of the lungs (visually confirmed). An experiment was setup in which parts of fissures were automatically removed to simulate the fissures being incomplete. The experiment was performed for each lung, for each fissure separately. The setup of the experiment was as follows: for a scan with complete fissures, the fissure was automatically segmented as described in Section III. Since fissures are most often incomplete at the hilum [3], [21], a part of the fissure was automatically removed from the hilum inward as follows: A sphere was defined with the carina as the center point. The radius of the sphere was chosen to contain exactly the desired part of the ground truth fissure to be removed. Next, all voxels inside the sphere were set to zero in the fissure enhancement result. Since the lobe segmentation method does not use the original CT data, it does not benefit in any way from the fact that the fissure is actually complete. For the experiment, $10\%, 20\%, \ldots, 70\%$ of the fissures were removed. Both for the left and the right lung, six of the scans in test set A showed complete fissures and were used for this experiment. The mean distance between the manually defined fissures and the automatically determined lobe border was used as an evaluation measure. Since the manually drawn fissures are complete, they provide a segmentation of the actual lobe borders. Examples of the simulated incomplete fissures can be seen in Fig. 7. To compare the performance of the method with our previously published lobe segmentation method [13] in cases with incomplete fissures, experiment 2 was repeated using the method proposed in [13] (experiment 2b).
3) To investigate the contribution of using the approximated lobe borders from the bronchial tree to guide the lobe segmentation, the second experiment was repeated with two different settings for the weights ω_f, ω_l, and ω_b. The settings used are given in Table I. The first setting (experiment 3a), does not take into account the approximated lobe border from the bronchial tree when the fissures are incomplete. In the second setting (experiment 3b) the fissures are not taken into account, and lobe segmentation is only based on the lungs and the approximated lobe border from the bronchial tree.
4) The lobe segmentations in the 100 scans from test set B were evaluated using a scoring system similar to the eval-

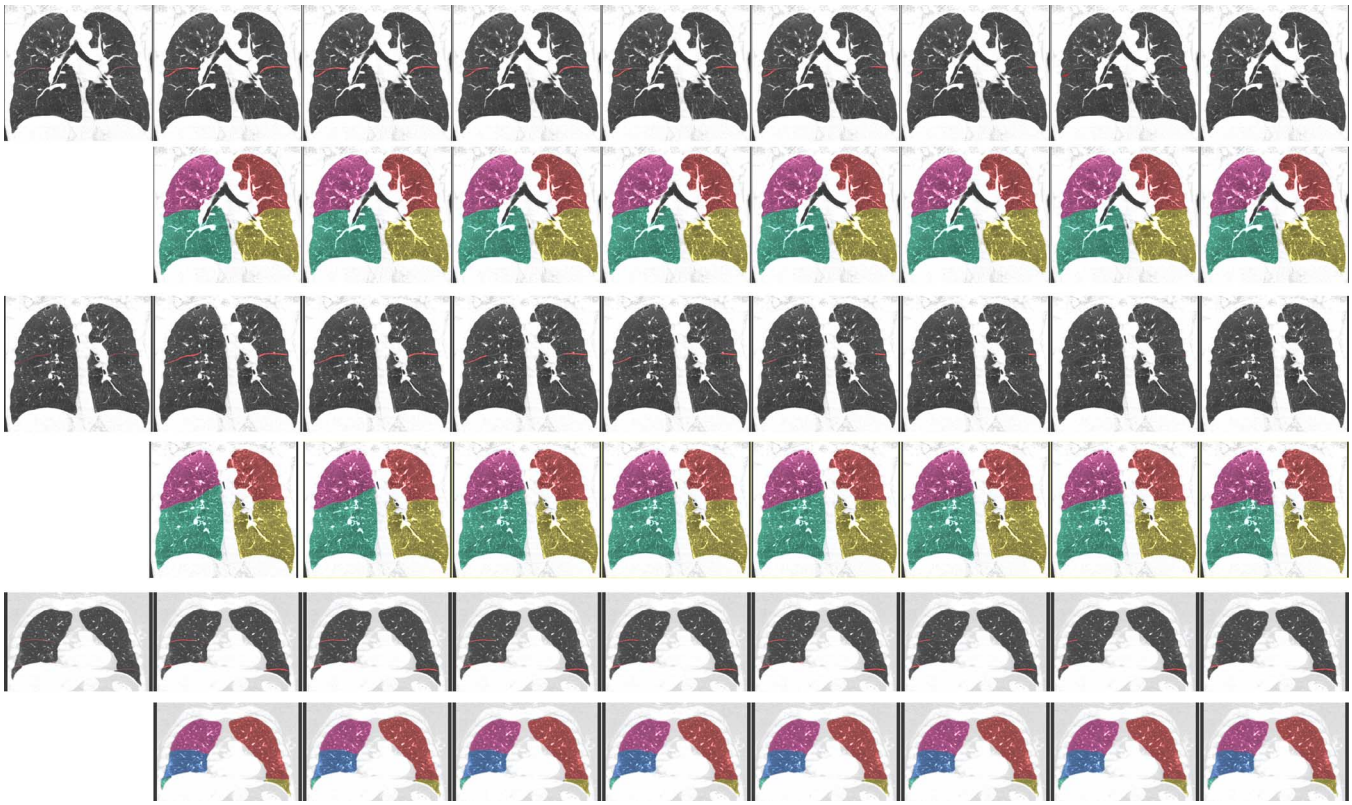

Fig. 7. Three examples of the results of experiment 2, in which parts of fissures were automatically removed to test the robustness of the automatic lobe segmentation in the presence of incomplete fissures. The first two examples are taken from scans in which parts of the right and left major fissures were removed, the last example is an example where the minor fissure was removed. The first frame of the first, third, and fifth row show the ground truth, the next frame shows the automatically detected fissures when no part of the fissures was removed, the third frame shows the fissures with 10% removed. In the fourth frame, the fissures with 20% removed are shown. The remaining frames show the fissures with $30\%, 40\%, \ldots 70\%$ removed. Note that the removal is 3-D, so the percentages do not necessarily reflect what is seen in this 2-D slice. In the second, fourth, and sixth row the corresponding lobe segmentations are provided.

uation described in [12]. The following numeric scoring system was applied.

- 5: Excellent segmentation and extrapolation of the fissures.
- 4: Segmentation error within 12 mm of the true lobe border.
- 3: Segmentation error further than 12 mm of the true lobe border. Lobe segmentation still useable.
- 2: Numerous or large segmentation errors, usefulness of segmentation in doubt.
- 1: Unusable segmentation.

Contrary to the procedure outlined in [12], the scoring was applied to all three lobe borders separately, including the minor fissure in the right lung, which was not evaluated in [12]. In addition, in [12] segmentation errors were defined by lobe borders crossing vessels or hilar vessels. Such failures proved extremely rare in our lobe segmentation, therefore, the evaluation was made more strict and quantitative. Four bands around the automatically determined lobe borders were shown with a width of 3 mm. If the true lobe border, as judged by a radiologist, was within the first band of 3 mm around the automatic lobe border, a score of 5 was given. If the score of the observer was lower than 5, the observer was asked to judge in which of the bands around the automatic lobe border the actual lobe border should be. This allows for a quantitative evaluation with a precision of 3 mm. Since the evaluation is about lobe borders where no fissure is present, evaluations on submillimeter level are not feasible.

TABLE I
SETTINGS OF THE WEIGHTS ω_l, ω_f, AND ω_b FOR THE DIFFERENT EXPERIMENTS

weight	exp 2	exp 3a	exp 3b
ω_f	4	4	0
ω_l	1	1	1
ω_b	1	0	1

The results of this evaluation are a score for each fissure for each scan and a quantification of the errors found. The results are presented per lobe border for the complete test set B.

VII. RESULTS

Table II provides the results of experiment 1. In Fig. 6 examples of the automatic lobe segmentation and the manual fissure segmentation are shown. It can be seen in both Table II and Fig. 6 that the automatic lobe segmentation closely follows the fissures.

The results of experiment 2, in which part of the fissures were removed to the test robustness of the method against different levels of incomplete fissures, are provided in Table III. The mean distance of the manually segmented complete fissure to the automatic lobe border is provided for each percentage

TABLE II
RESULTS OF EXPERIMENT 1. RMS, MEAN, AND MAXIMUM DISTANCE FROM THE MANUALLY DRAWN FISSURE TO THE AUTOMATICALLY FOUND LOBE BORDER FOR TEST SET A

Fissure	rms(mm)	mean (mm)	max (mm)
left major	1.28 ± 0.37	0.48 ± 0.15	10.3 ± 3.52
right major	1.88 ± 0.27	1.23 ± 0.24	9.96 ± 2.89
right minor	1.98 ± 0.96	1.28 ± 0.53	9.59 ± 7.38

TABLE III
RESULTS OF EXPERIMENT 2 AND 3 AS DESCRIBED IN SECTION VI. MEAN DISTANCE (MM) FROM THE MANUALLY DRAWN LOBE BORDER (COMPLETE FISSURE) TO THE AUTOMATICALLY FOUND LOBE BORDER FOR DIFFERENT PERCENTAGES OF THE FISSURE REMOVED ARE PROVIDED FOR THE DIFFERENT SETTINGS. THE ROWS INDICATE WHICH FISSURE IS EVALUATED, THE COLUMNS PROVIDE THE RESULTS FOR 0% TO 70% REMOVED

fissure	**0%**	**10%**	**20%**	**30%**	**40%**	**50%**	**60%**	**70%**
	exp. 2: ω_f = 4, ω_l = 1, ω_b =1							
left major	0.51	0.54	0.63	0.70	0.93	1.10	1.58	1.81
right major	1.22	1.32	1.54	1.79	2.18	2.56	3.22	3.71
right minor	1.08	1.02	1.37	2.00	2.60	3.38	4.61	5.90
	exp. 3a: ω_f = 4, ω_l = 1, ω_b =0							
left major	0.52	0.59	0.83	0.94	1.17	1.64	3.02	3.94
right major	1.25	1.39	1.70	2.13	2.83	3.76	5.28	7.31
right minor	1.08	1.07	1.61	2.30	3.21	4.15	6.56	8.06
	exp. 3b: ω_f = 0, ω_l = 1, ω_b =1							
left major	4.52	4.52	4.52	4.52	4.52	4.52	4.52	4.52
right major	6.33	6.33	6.33	6.33	6.33	6.33	6.33	6.33
right minor	6.23	6.23	6.23	6.23	6.23	6.23	6.23	6.23

TABLE IV
RESULTS OF EXPERIMENT 2B AS DESCRIBED IN SECTION VI. MEAN DISTANCE (MM) FROM THE MANUALLY DRAWN LOBE BORDER (COMPLETE FISSURE) TO THE AUTOMATICALLY FOUND LOBE BORDER USING THE LOBE SEGMENTATION METHOD AS DESCRIBED IN [13]ARE PROVIDED. THE ROWS INDICATE WHICH FISSURE IS EVALUATED, THE COLUMNS PROVIDE THE RESULTS FOR 0% TO 70% REMOVED

fissure	**0%**	**10%**	**20%**	**30%**	**40%**	**50%**	**60%**	**70%**
left major	0.48	1.05	1.89	2.69	3.33	12.72	12.55	14.45
right major	2.19	2.65	3.48	3.68	4.62	5.06	5.92	7.97
right minor	9.06	10.02	10.49	11.00	11.47	13.46	15.53	18.77

of fissure voxels removed. The performance of the automatic method gradually decreases when a larger percentage of the fissure is removed. Examples of the results of experiment 2 are shown in Fig. 7.

The results of experiment 2b, in which a previously proposed lobe segmentation method was applied to the scans in which part of the fissures were removed, are provided in Table IV. By comparing the results from experiment 2b to the results of experiment 2 it can be seen that the difference between the two methods becomes more pronounced with increasing incompleteness of the fissures. Fig. 8 shows an example of the results both methods for one slice, for 10% and 40% of the fissures removed.

In Table III the results of experiment 3 are provided. The mean distance from the manually drawn lobe border (complete fissure) to the automatically found lobe border is provided for each setting, for each percentage of fissure removed. Note that for experiment 3b the fissures are not used as input, therefore, the result is the same for each percentage of fissure removed. From Table III, it can be seen that adding the approximated lobe border from the bronchial tree during the registration improves the segmentation result when fissures are incomplete.

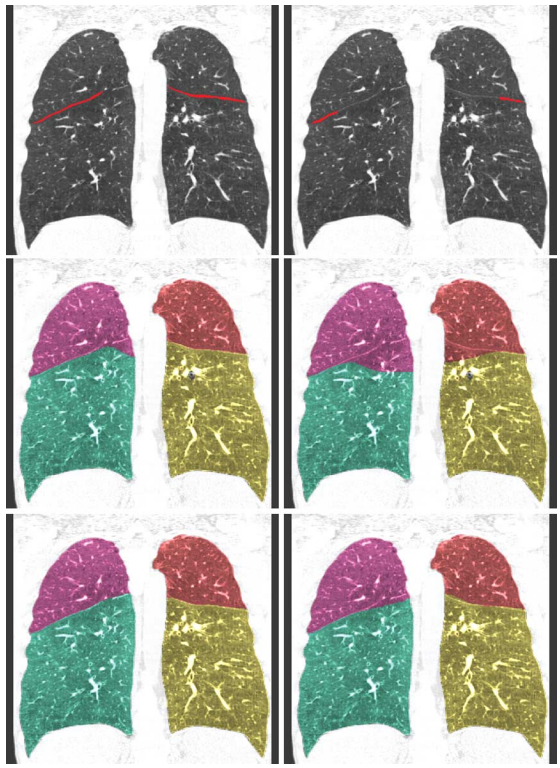

Fig. 8. An example result of experiment 2b, in which parts of the fissures were automatically removed to test the robustness of the automatic lobe segmentation proposed in [13] in the presence of incomplete fissures. The first row shows a coronal slice with 10% and 40% of the fissures removed. The second row shows the results of the method from [13] for the respective slices. In the last row the results of the method proposed in this paper on the same slices are shown. It can be seen that the previously proposed method closely follows the fissure where present, but where no fissure is present the lobe border is extended in an anatomically implausible manner.

TABLE V
RESULTS OF EXPERIMENT 4, IN WHICH AN OBSERVER STUDY ON THE 100 LOW DOSE SCANS WITH INCOMPLETE FISSURES FROM TEST SET B WAS PERFORMED. THE AVERAGE SCORE AS WELL AS THE DIVISION OVER THE DIFFERENT SCORES IS PROVIDED FOR EACH LOBE BORDER SEPARATELY

	left major	right major	right minor
average score	4.6	4.8	4.6
% score 5	79	89	76
% score 4	12	8	18
% score 3	9	3	4
% score 2	0	0	2
% score 1	0	0	0

The results of experiment 4 are provided in Table V. When a score of 4 was given (error within 12 mm of the true lobe border) the average error was 6–9 mm from the true lobe border. Results on scans with incomplete fissures from test set B are shown in Fig. 9. There were 55 scans for which all three fissures received a score of 5. For 85 scans all fissures were scored with a 4 or higher, 98 scans received a score higher than or equal to 3 for all fissures. Finally, the last two scans received a score of 2 for the minor fissures, the major fissures in both those scans received a score of 5.

VIII. DISCUSSION AND CONCLUSION

Complete pulmonary fissures are rare, which makes automatic lobe segmentation challenging due to the absence of a

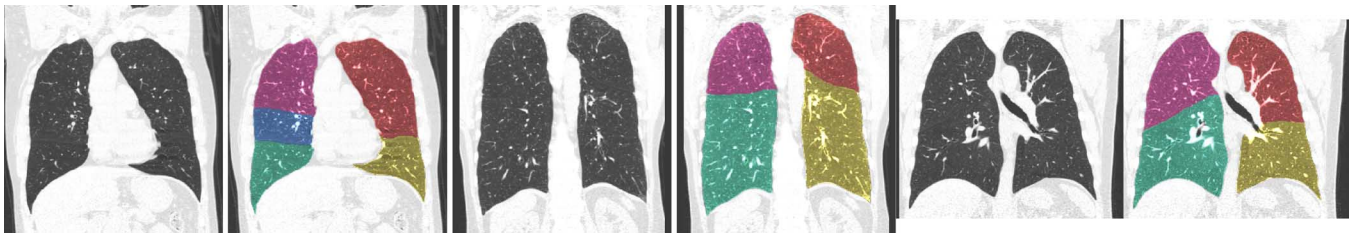

Fig. 9. Example output of the results on test set B. The original image and the lobe segmentation result are shown for three images. The first example shows a scan for which the minor fissure in the right lung is absent (visually judged by the radiologist during the observer study). The major fissures in both lungs are also incomplete in 3-D. The second example shows a scan for which the right major fissure is incomplete, and completely missing in the top of the lung. In the last example a slice of a scan in which all three fissures were incomplete is shown. The score from experiment 4 for all three images shown here was 5.

physical border. Automatic lobe segmentation in the presence of incomplete fissures has not received much attention in literature so far. In this paper, an automatic lobe segmentation method was presented that was especially designed to be able to handle both complete and incomplete fissures. The method was evaluated on two test sets of 120 scans in total. The results showed that if a fissure was present, the lobe borders were on average within 1 mm of the manual reference standard. For cases with incomplete fissures, a radiologist scored the automatic lobe border to be within 12 mm of the true lobe border for 94% of the lobe borders on average. For only two cases, the lobe border of the right minor fissure was found to be of doubtful quality.

To evaluate the robustness and performance of the automatic lobe segmentation method for different percentages of incompleteness of fissures, a simulated experiment on scans with complete fissures was performed. By removing parts of the fissures that are used as input for the automatic lobe segmentation method, incomplete fissures were mimicked. The results showed that both quantitatively and visually the method performed very well. Even when 70% of the fissures was removed, the automatically extracted lobe border was on average still within 4 mm of the real lobe border for the major fissures and within 6 mm for the right minor fissure. The accuracy gradually decreases when fewer fissures are present. Fig. 7 shows that the lobe segmentation remains similar to the lobe segmentation with complete fissures even after removing 70% of the fissure.

A limitation of the simulations as performed for experiment 2 is that the incomplete fissures are simulated from scans with complete fissures. In practice, the fissures can be incomplete for two reasons: by nature or due to pathological processes. In the latter case, the morphology of the lobar boundary might be different than the morphology of subjects with complete fissures.

The results of experiment 2b provided in Table IV show that the lobe segmentation method proposed in [13] is able to perform equally well for the major fissures in cases with (nearly) complete fissures. However, when the fissures are incomplete the performance quickly deteriorates. This is illustrated in Fig. 8, where it can be seen that the result of the previously proposed lobe segmentation deteriorates substantially when a (substantial) part of a fissure is missing. These results illustrate the need for the proposed lobe segmentation method.

The rationale behind the method presented in this paper is intuitive and similar to the methodology humans use when segmenting lobes manually. When the fissures are complete, they define the lobe borders, but where no fissure is present, knowledge about the shapes of the various lobes as well as anatomical information, such as the bronchial tree, are used. An assumption of the method presented in this paper is that adding the approximated lobe borders from the bronchial tree in cases with incomplete fissures improves the segmentation results. To test the validity of this assumption, two experiments were performed. In experiment 3a, the approximated lobe border from the bronchial tree was not included, only lung and fissure segmentations were used during registration. In experiment 3b, only the approximated lobe borders and the lungs were employed as input to the registration. The results provided in Table III admit of two conclusions. First, that using only the approximated lobe border from the bronchial tree provides a reasonable approximation of the true lobe borders, indicating that the approximated lobe borders provide useful information. And second, that adding the bronchial tree information to the automatic lobe segmentation, next to the lungs and fissures, improves segmentation results in cases with incomplete fissures.

Next to the simulated experiment, a qualitative and quantitative evaluation were performed on 100 low dose scans from a lung cancer screening trial. The scans were specifically selected to have at least one incomplete fissure. The results show that a radiologist judges the automatic lobe segmentation for the cases with incomplete fissures to be correct in 79% of the cases for the left lung, and in 89% and 76% of the cases for the major and minor lobe borders in the right lung. In the cases where an error smaller than 12 mm was detected, the error was on average within 6–9 mm of the true lobe border. Due to the setup of the experiment, the scoring is expected not to suffer from large interobserver variability.

It is important to realize the difficulty of the task of lobe segmentation in cases with incomplete fissures. The scans in test set B were selected to have substantially incomplete fissures, this can also be appreciated in the examples in Fig. 9. In those cases, it is also difficult for radiologists to indicate the actual lobe borders. The evaluation did not only show that the automatic segmentation performed well in the majority of cases, but also that for only two cases, for only one lobe border, the radiologist judged the segmentation quality as doubtful. In those two cases, the minor fissure was completely absent. The other two lobe borders in those scans were both scored as 5 (correct segmentation) in both scans. An indication of the difficulty of

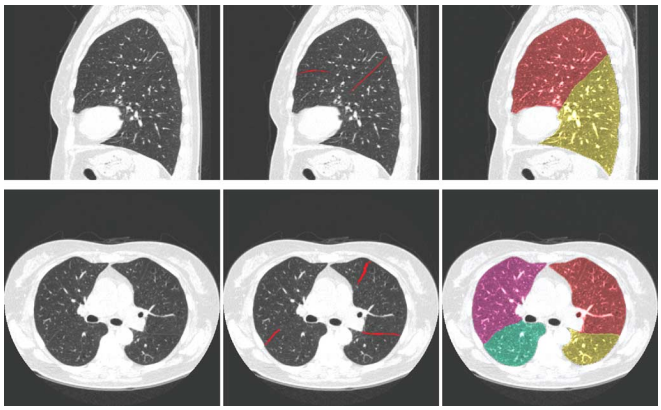

Fig. 10. Example output of a scan from test set B in which an accessory fissure was detected by the fissure segmentation step. The first row shows an original sagittal slice in the first frame, the fissure segmentation in the second frame, and the lobe segmentation in the third frame. The second row shows the same images for an axial slice.

the task are the results reported in [12], where in a similar evaluation for scans with incomplete fissures 40% of the scans were judged to have a correct lobe segmentation.

The lobe segmentation method presented in this paper relies on the success of the automatic segmentations of the lungs, fissures, and bronchial tree. When one of those segmentations fails, the method is likely to perform worse. This is illustrated in experiments 3a and 3b, in which the fissure and bronchial tree segmentations are left out. Although results deteriorate when input segmentations are missing, the method is relatively robust against this: Even when the fissure segmentation is completely missing, the automatic lobe borders are still within 6 mm on average of the true lobe borders.

Next to fissures being incomplete, false positive responses of the fissure detection, for example due to accessory fissures, scarring or fibrosis, might be present in the fissure segmentation. Fig. 10 shows an example of a scan from test set B in which an accessory fissure was present in the fissure segmentation. It can be seen that the lobe segmentation result did not deteriorate despite the additional fissure response being present. However, in case a false fissure response is present that has approximately the same position and orientation as one of the lobar fissures, the registration might be drawn to this fissure instead of the real lobar fissure. Such failures did not occur in the data used for this paper.

Next to the bronchial tree segmentation failing completely, it is possible that the segmentation of the bronchial tree contains errors. In those cases, the approximated lobar borders might be at the wrong location in the scan. It can be seen in Table III that this will influence the results in cases where the fissures are (substantially) incomplete. If the approximated lobar border from the bronchial tree is far from the (part of) the fissure that has been found, it is likely that the results will be similar to the results when the bronchial tree is not taken into account.

When all prerequisite segmentations are successful, the automatic lobe segmentation can still fail if a similar shape of the lobar borders in the test image is not represented in the atlases.

TABLE VI
AVERAGE COMPUTATION TIME ON A SINGLE CORE USING A 2.4-GHZ PROCESSOR PER SCAN FOR EACH STEP OF THE ALGORITHM

Operation	time
Lung segmentation	55 sec
Fissure segmentation	90 min
Airway lobe border segmentation	2 min
Preparation for registration	30 sec
Atlas selection	10 min
Accurate registration	15 min
Postprocessing	20 sec

This is likely to happen when only five atlases are used. The registration could be set to have more degrees of freedom such that the lobar borders can deform to any shape, but that could violate one of the main goals of the method; to deform lobe borders from scans with complete fissures in an anatomically plausible way. A solution would be to manually (or semi-automatically) segment the lobes in such a scan and add it to the set of atlases to make sure that if a similar shape is encountered, the method is able to segment the lobes automatically.

The method presented in this paper takes on average 2 h per scan on a single core. Table VI shows the computational time needed for each step of the algorithm. It can be seen that the fissure segmentation is the most computationally expensive part of the algorithm, taking 75% of the computation time. The method does not rely specifically on the fissure segmentation algorithm used in this paper. A faster fissure segmentation method could be plugged in, especially since the algorithm has been shown to work well even when parts of the fissures are missing. Two other steps of the method that are time consuming are the atlas selection and the accurate registration. This is due to the registration settings used; a setting was chosen that performed well in pilot experiments without optimizing for speed. Especially the accurate registration can be faster. In addition, the fissure segmentation and atlas selection are easy to parallelize.

An important subject for future research is the performance of the automatic lobe segmentation in cases with COPD, interstitial lung disease, or other abnormalities that change the appearance of the lung parenchyma and the morphology of the lobe borders. In the data used in this paper, mild to moderate emphysema was present, which did not influence the results of the lobe segmentation. It is expected that in the presence of severe abnormalities the results will deteriorate due to failures of one or more of the prerequisite segmentations or lobar shapes that are not represented in the set of atlases.

In summary, an automatic lobe segmentation method was presented that is robust against incomplete fissures, which occur frequently. The method was evaluated on two test sets of 120 scans in total and shown to perform well in the presence of incomplete fissures.

REFERENCES

[1] B. N. Raasch, E. W. Carsky, E. J. Lane, J. P. O'Callaghan, and E. R. Heitzman, "Radiographic anatomy of the interlobar fissures: A study of 100 specimens," *Am. J. Roentgenol.*, vol. 138, no. 6, pp. 1043–1049, 1982.

[2] A. Aziz, K. Ashizawa, K. Nagaoki, and K. Hayashi, "High resolution CT anatomy of the pulmonary fissures," *J. Thoracic Imag.*, vol. 19, no. 3, pp. 186–191, 2004.

[3] M. Gülsün, O. M. Ariyürek, R. B. Cömert, and N. Karabulut, "Variability of the pulmonary oblique fissures presented by high-resolution computed tomography," *Surgical Radiologic Anatomy*, vol. 28, no. 3, pp. 293–299, 2006.

[4] R. A. Maxfield, "New and emerging minimally invasive techniques for lung volume reduction," *Chest*, vol. 125, no. 2, pp. 777–783, 2004.

[5] "National Emphysema Treatment Trial Research Group, "Patients at high risk of death after lung-volume-reduction surgery"," *New Eng. J. Med.*, vol. 345, no. 15, pp. 1075–1083, 2001.

[6] J. Wang, M. Betke, and J. P. Ko, "Pulmonary fissure segmentation on CT," *Med. Image Anal.*, vol. 10, no. 4, pp. 530–547, 2006.

[7] E. M. van Rikxoort, B. van Ginneken, M. Klik, and M. Prokop, "Supervised enhancement filters: Application to fissure detection in chest CT scans," *IEEE Trans. Med. Imag.*, vol. 27, no. 1, pp. 1–10, Jan. 2008.

[8] J. Pu, B. Leader, J. K.Zheng, F. Knollmann, C. Fuhrman, F. C. Sciurba, and D. Gur, "A computational geometry approach to automated pulmonary fissure segmentation in CT examinations," *IEEE Trans. Med. Imag.*, vol. 28, no. 5, pp. 710–719, May 2009.

[9] J.-M. Kuhnigk, V. Dicken, S. Zidowitz, L. Bornemann, B. Kuemmerlen, S. Krass, H.-O. Peitgen, S. Yuval, H.-H. Jend, W. S. Rau, and T. Achenbach, "New tools for computer assistance in thoracic CT Part 1. Functional analysis of lungs, lung lobes and bronchopulmonary segments," *Radiographics*, vol. 25, no. 2, pp. 525–536, 2005.

[10] L. Zhang, E. A. Hoffman, and J. M. Reinhardt, "Atlas-driven lung lobe segmentation in volumetric X-ray CT images," *IEEE Trans. Med. Imag.*, vol. 25, no. 1, pp. 1–16, Jan. 2006.

[11] J. Pu, B. Zheng, J. K. Leader, C. Fuhrman, F. Knollmann, A. Klym, and D. Gur, "Pulmonary lobe segmentation in CT examinations using implicit surface fitting," *IEEE Trans. Med. Imag.*, vol. 28, no. 12, pp. 1986–1996, Dec. 2009.

[12] S. Ukil and J. M. Reinhardt, "Anatomy-guided lung lobe segmentation in X-ray CT images," *IEEE Trans. Med. Imag.*, vol. 28, no. 2, pp. 202–214, Feb. 2009.

[13] E. M. van Rikxoort, B. de Hoop, S. van de Vorst, M. Prokop, and B. van Ginneken, "Automatic segmentation of pulmonary segments from volumetric chest CT scans," *IEEE Trans. Med. Imag.*, vol. 28, no. 4, pp. 621–630, Apr. 2009.

[14] E. M. van Rikxoort, B. de Hoop, M. A. Viergever, M. Prokop, and B. van Ginneken, "Automatic lung segmentation from thoracic computed tomography scans using a hybrid approach with error detection," *Med. Phys.*, vol. 36, no. 7, pp. 2934–2947, 2009.

[15] S. N. Kalitzin, J. J. Staal, B. M. ter Haar Romeny, and M. A. Viergever, "A computational method for segmenting topological point sets and application to image analysis," *IEEE Trans. Pattern Anal. Mach. Intell.*, vol. 23, no. 5, pp. 447–459, May 2001.

[16] B. van Ginneken, W. Baggerman, and E. M. van Rikxoort, "Robust segmentation and anatomical labeling of the airway tree from thoracic CT scans," in *Med. Image Computing Computer-Assisted Intervent.*, 2008, vol. 5241, pp. 219–226.

[17] S. Klein, M. Staring, K. Murphy, M. A. Viergever, and J. P. W. Pluim, "elastix: A toolbox for intensity-based medical image registration," *IEEE Trans. Med. Imag.*, vol. 29, no. 1, pp. 196–205, Jan. 2010.

[18] S. Klein, M. Staring, and J. P. W. Pluim, "Evaluation of optimization methods for nonrigid medical image registration using mutual information and B-splines," *IEEE Trans. Image Process.*, vol. 16, no. 12, pp. 2879–2890, Dec. 2007.

[19] C. R. Maurer Jr., R. Qi, and V. Raghavan, "A linear time algorithm for computing exact euclidean distance transforms of binary images in arbitrary dimensions," *IEEE Trans. Pattern Anal. Mach. Intell.*, vol. 25, no. 2, pp. 265–270, Feb. 2003.

[20] D. M. Xu, H. Gietema, H. de Koning, R. Vernhout, K. Nackaerts, M. Prokop, C. Weenink, J. Lammers, H. Groen, M. Oudkerk, and R. van Klaveren, "Nodule management protocol of the NELSON randomised lung cancer screening trial," *Lung Cancer*, vol. 54, no. 2, pp. 177–184, 2006.

[21] M. Mahmut and H. Nishitani, "Evaluation of pulmonary lobe variations using multidetector row computed tomography," *J. Comput. Assit. Tomogr.*, vol. 31, no. 6, pp. 956–960, 2007.